applied sciences

MDPI

Article

Boron Neutron Capture Therapy: Microdosimetry at Different Boron Concentrations

Valeria Conte *, Anna Bianchi and Anna Selva

Istituto Nazionale di Fisica Nucleare INFN, Laboratori Nazionali di Legnaro, Viale dell'Università 2, 35020 Legnaro, Italy; anna.bianchi@lnl.infn.it (A.B.); anna.selva@lnl.infn.it (A.S.)
* Correspondence: valeria.conte@lnl.infn.it

Featured Application: Application of microdosimetric techniques to characterize the mixed radiation field in boron neutron capture therapy.

Abstract: This paper explores the role of microdosimetry in boron neutron capture therapy (BNCT), a cancer treatment involving the selective accumulation of boron-containing compounds in cancer cells, followed by neutron irradiation. Neutron interactions with ^{10}B induces a nuclear reaction, releasing densely ionizing particles, specifically alpha particles and recoiling lithium-7 nuclei. These particles deposit their energy within a small tissue volume, potentially targeting cancer cells while sparing healthy tissue. The microscopic energy distribution, subject to significant fluctuations due to the short particle range, influences treatment efficacy. Microdosimetry, by studying this distribution, plays a crucial role in optimizing BNCT treatment planning. The methodology employs paired tissue equivalent proportional counters (TEPCs), one with cathode walls enriched with boron and the other without. Precise assessment of boron concentration is essential, as well as the ability to extrapolate results to the actual ^{10}B concentration within the treatment region. The effective ^{10}B concentrations within four boronated TEPCs, containing 10, 25, 70, and 100 ppm of ^{10}B, have been determined. Results show variations of less than 3% from nominal values. Additionally, dose enhancement due to BNC interactions was measured and found to be proportional to the ^{10}B concentration, with a proportionality factor of 7.7×10^{-3} per ppm of boron. Based on these findings, a robust procedure is presented for assessing the impact of BNCT in the treatment region, considering potential variations in boron content relative to the TEPC used.

Keywords: radiation therapy; BNCT; microdosimetry

Citation: Conte, V.; Bianchi, A.; Selva, A. Boron Neutron Capture Therapy: Microdosimetry at Different Boron Concentrations. *Appl. Sci.* **2024**, *14*, 216. https://doi.org/10.3390/app14010216

Academic Editor: Zhonghua Sun

Received: 5 December 2023
Revised: 21 December 2023
Accepted: 23 December 2023
Published: 26 December 2023

1. Introduction

Boron neutron capture therapy (BNCT) is a unique radiotherapeutic approach for treating cancer, relying on the ^{10}B(n, α)^{7}Li nuclear reaction when stable ^{10}B interacts with thermal neutrons. The possibility of exploiting the neutron capture reaction to treat tumors was introduced by Locher in 1936, laying the foundation for the development of boron neutron capture therapy (BNCT) [1]. The first application of BNCT took place in 1951, targeting a patient with malignant glioma. This groundbreaking endeavor utilized the existing nuclear research reactor at the Brookhaven Graphite Research Reactor [2]. A comprehensive overview of the state of BNCT based on reactor sources of neutrons was provided in a technical document published by the International Atomic Energy Agency in 2001 [3]. More recent advances in the field are summarized in a new IAEA report, published in 2023 [4].

BNCT is particularly promising for treating locally invasive malignant tumors due to the high neutron-capture cross-section of ^{10}B and the short ranges of its resulting alpha particles and recoiling ^{7}Li nuclei [1]. These high linear energy transfer (LET) particles, with LET values of approximately 150 keVμm^{-1} for alpha particles and 175 keVμm^{-1} for ^{7}Li

nuclei, deposit their energy within a small tissue volume, typically within micrometers. This selective energy deposition offers potential precision in cancer cell destruction while sparing surrounding healthy tissue. The alpha particles and ^{7}Li nuclei have approximate ranges of 4.5 μm and 10 μm [3,4].

The key advantage of BNCT lies in the selective uptake of boron-loaded carriers by cancer cells, ensuring a higher concentration of boron atoms in cancerous tissue compared to healthy tissue. This selective uptake enables additional doses from alpha and lithium particles, effectively sterilizing cancer cells while limiting damage to healthy tissue [5].

BNCT presents several dose components, including the 'boron dose' (alpha and lithium-ion disintegration products), fast neutron dose, nitrogen capture proton dose, and gamma doses from the neutron source and from capture and scattering of neutrons in the beam line structures, as well as those produced in the body from hydrogen capture reactions. Accurate dosimetry in BNCT is essential due to its various radiation components. It is also essential to minimize radiation components other than those from thermal neutrons [3,4].

Microdosimetry, involving the measurement of various components contributing to the total dose [6,7], has emerged as a promising tool for characterizing radiation field quality in BNCT. The first measurements were conducted in 1992 [6] and subsequently discussed in a review paper [7]. Since then, both Monte Carlo simulation studies [8,9] and experimental measurements using tissue-equivalent proportional counters (TEPCs) have explored microdosimetry in the context of reactor-based BNCT [10–16] and accelerator-based BNCT [17].

Given the diverse aspects of the investigated radiation fields (gamma component, fast neutron component, epithermal/thermal neutron field) and the variations in the employed detectors (different sensitive volume shape, simulated site size, and boron concentration, etc.), the literature microdosimetric distributions are not directly comparable with those presented in this work. However, the measurements by Wuu, Kota, and Burmeister [6,10,11] were conducted at similar site sizes of 2, 0.5, and 1 μm, respectively; therefore, the pure BNC component is expected to be similar to ours.

No measurement has been reported for variable boron concentrations to date. The dose resulting from the boron neutron capture (BNC) reaction is directly proportional to the concentration of ^{10}B. Therefore, adjusting the dose measurement to different concentrations of ^{10}B allows for a more accurate simulation of the realistic situation in the tumor and surrounding healthy tissue.

This study aims to deepen our understanding of boron neutron capture therapy (BNCT) by achieving the following objectives: (1) Verification of the nominal ^{10}B concentration. (2) Optimization of the procedure for determining the BNC component through pairwise microdosimetric measurements. (3) Calculation of the BNC component for varying ^{10}B concentrations.

To accomplish these goals, we utilized a cylindrical tissue-equivalent proportional counter (TEPC) equipped with interchangeable cathode walls doped with ^{10}B atoms at different concentrations (0, 10, 25, 70, and 100 ppm) [18]. Experimental measurements were conducted at the LNL-INFN accelerator-based BNCT facility available at the Legnaro National Laboratories of the Italian National Institute for Nuclear Physics (LNL-INFN). This is a research-oriented facility capable of delivering a thermal neutron flux of about 4.5×10^{5} s^{-1}cm^{-2} [17,19].

2. Materials and Methods

2.1. The Experimental Setup

The measurements were conducted at the MUNES thermal neutron source, located along the +15° beam line of the CN accelerator at LNL. This source generates neutrons through the ^{9}Be(p,n)^{9}B reaction, employing a 5 MeV proton beam directed at a beryllium–vanadium target. The fast neutron spectrum, characterized by a maximum neutron energy of approximately 3.2 MeV [20], is tailored to the thermal energy range using a large beam-shaping assembly (BSA) composed of 4014 kg of graphite, 88.5 kg of heavy water, 53 kg of

PFTE, and 24 kg of bismuth. The BSA, occupying a volume of about 3 m^3, facilitates the production of thermal neutrons, which are extracted through a bismuth exit channel with a surface area of 10 cm × 10 cm (refer to Figure 1). For further details on the MUNES thermal neutron facility, additional information can be found in [17,19].

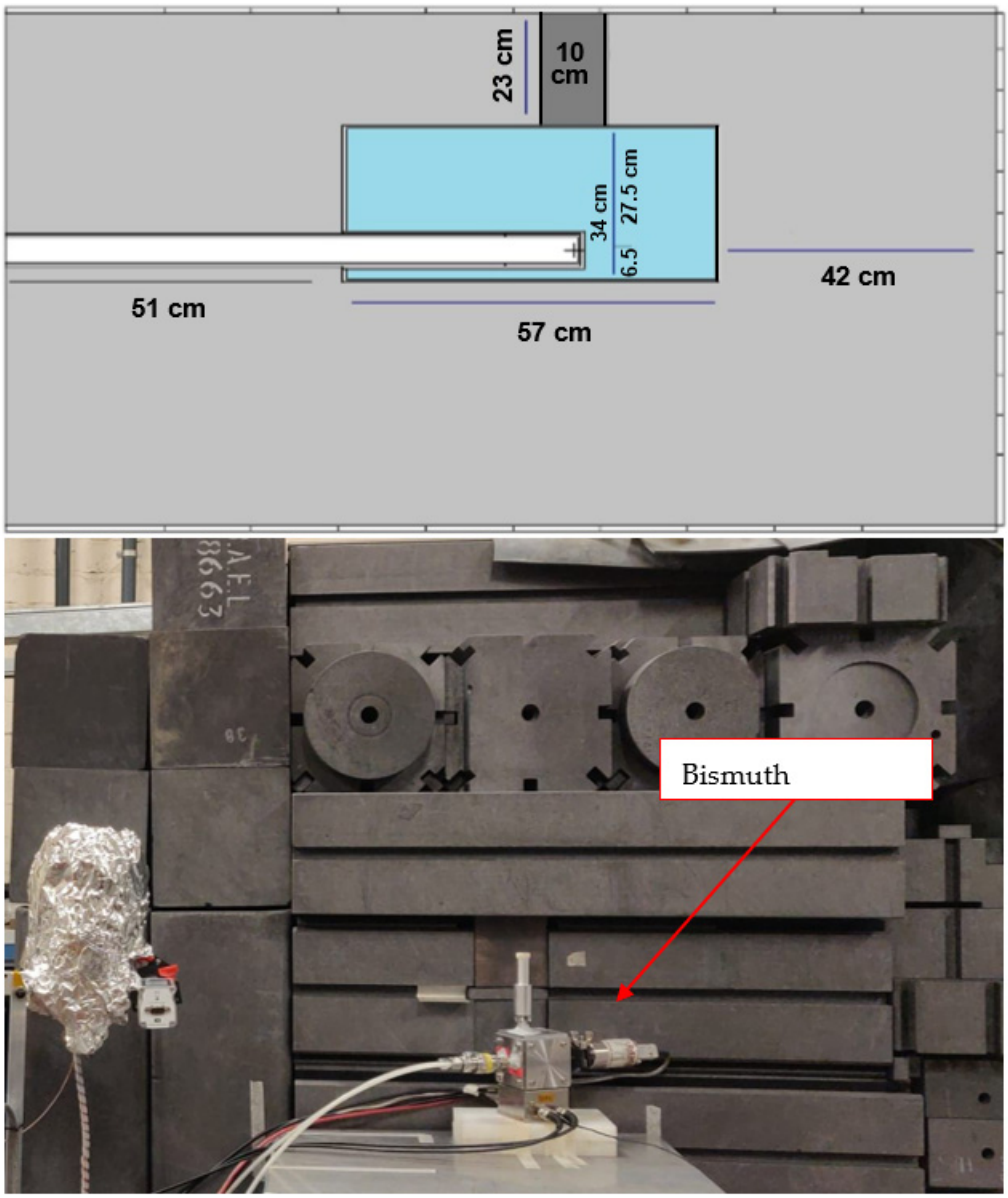

Figure 1. Top panel: top view drawing of the moderator. Heavy water (light blue), graphite (grey), and bismuth (dark grey). The white region is the beam line that enters the moderator. **Bottom panel**: a picture of the irradiation set-up with the BSA for thermal neutrons and the TEPC in front of the bismuth window.

2.2. Microdosimetric Measurements Using TEPC

Microdosimetric investigations were performed using a tissue-equivalent proportional counter (TEPC) of cylindrical shape, which was designed and constructed at LNL. The sensitive volume of the TEPC consists of a cavity featuring equal diameter and height of 1.3 cm. The anode is made of a 100 µm gold-plated tungsten wire and is surrounded by a helix, made of the same wire, with a diameter of 6 mm. This helix confines the electronic avalanche in proximity to the anode. The cathode wall has a thickness of 1 mm and is made of A-150 tissue-equivalent plastic. It is designed as two half-cylindrical shells that

can be removed and replaced without difficulty (Figure 2). This feature allows the counter to be supplied with cathode walls doped with different concentrations of boron. For the current measurements, five different concentrations of boron were used, using five pairs of half-shells. The boron concentrations utilized were 0, 10, 25, 70, and 100 ppm of ^{10}B. The TEPC is enclosed within an aluminum cap with a thickness of 0.2 mm. The total counter thickness is 0.21 g/cm^2. The anode, helix, and cathode electrodes can be independently biased to improve gas gain and energy resolution. Additional information on the operation of this type of TEPC can be found in reference [18].

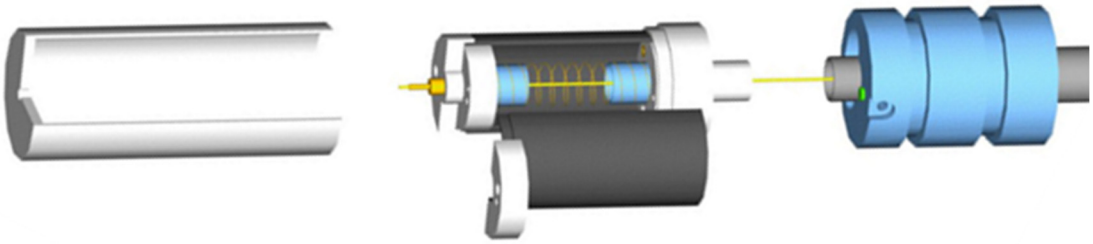

Figure 2. A 3D rendering of the TEPC with coaxial helix for avalanche confinement and interchangeable cathode walls.

Pure propane gas was used to fill the cylindrical cavity of the TEPC. The gas pressure was set at 31.4 hPa, which provided a tissue-equivalent diameter of 1 µm [21]. To ensure stable gas gain, the gas continuously flowed at a rate of 0.1 cc/min STP. The cathode bias voltage was set at −210 V, the helix at −200 V, and the anode at +340 V. Five independent measurements were conducted using the same TEPC. The first measurement involved undoped cathode walls, and the subsequent measurements used the other four sets of cathode walls loaded with different concentrations of ^{10}B. The detector was placed in the same irradiation position in front of the bismuth window (Figure 1), and 10^6 counts were recorded for each measurement.

2.2.1. Data Acquisition and Processing

The charge induced by radiation in the sensitive volume (SV) and collected by the anode was fed to a low-noise charge-sensitive preamplifier (PA) specifically designed for this detector and constructed at LNL. The signal was then sent in parallel to two spectroscopy linear amplifiers, each with a different gain setting and a shaping time of 2 µs. The amplified signals were further processed using a dual-channel peak-detecting analog-to-digital converter (ADC), specifically the ORTEC Model ASPEC-MCA-927. To verify the linearity of the electronic circuitry, a high-precision pulse generator was employed.

2.2.2. Calibration of Lineal Energy

In microdosimetry, lineal energy (denoted as y) is defined as the ratio of the energy imparted (ε) by individual ionizing particles to the mean chord length ($\bar{l}$) of the SV. Lineal energy distributions are often used to describe radiation quality. Higher lineal energy values indicate a greater probability of localized energy deposition, which can lead to more severe biological effects. The unit of lineal energy is usually expressed in keV/µm.

$$y = \frac{\varepsilon}{\bar{l}} \tag{1}$$

Microdosimetry deals with two probability density functions, namely the frequency distribution, $f(y)$, and the dose distributions, $d(y)$, which are related by the following equation:

$$d(y) = \frac{yf(y)}{\int_0^\infty yf(y)dy} \tag{2}$$

More details on microdosimetric variables and distributions can be found in [22]. In this study, we calibrated the lineal energy distributions using the electron-edge technique. We assigned the value of 10.8 keV/µm to the flex position of the fitted Fermi function, following the methodology outlined in the work by Bianchi et al. [23].

To account for environmental noise conditions, the detection threshold was set at approximately 0.3 keV/µm. Consequently, we linearly extrapolated the frequency distributions down to 0.01 keV/µm, as detailed in [24]. For a more comprehensive understanding of the methodology, please refer to [23,24].

2.2.3. Analysis of Microdosimetric Spectra and Dose Components

The analysis of microdosimetric spectra, illustrating dose distributions of lineal energy, was conducted based on the following considerations. In the case of indirectly ionizing radiation, such as photons and neutrons, energy deposition within the SV occurs primarily via secondary charged particles generated in the A-150 cathode, while the number of secondary charged particles generated in the gas is very small due the low density of the interacting medium. One example of such secondary particles is Compton electrons, contributing to events with small lineal energy, typically below 20 keV/µm, in the "photon-component" region (refer to Figure 3). The region of y-values greater than 20 keV/µm is produced mainly by protons and other recoil ions. These particles have higher stopping powers than electrons; therefore, they deposit greater amounts of energy within the SV. This region of the spectrum above 20 keV/µm is referred to as the "neutron component" and encompasses events arising from fast, epithermal, and thermal neutron reactions, including the contribution from BNC events when ^{10}B atoms are present. The BNC component occupies the spectrum region ranging from 50 to 800 keV/µm.

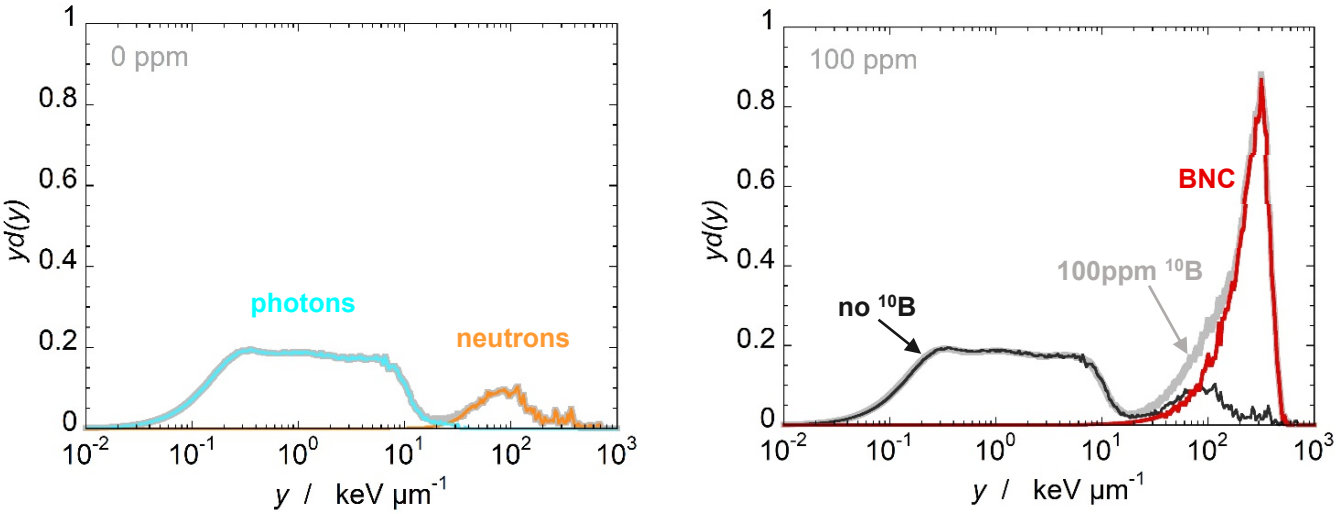

Figure 3. (**a**) Dose distributions of lineal energy without boron; (**b**) with a concentration of 100 ppm of ^{10}B. The relative contributions to the dose due to photons, neutrons, and pure BNC interactions are indicated. The BNC component is derived by subtracting the no ^{10}B curve from the photon-aligned 100 ppm ^{10}B curve. More details are provided in the text.

To determine the three main dose components, namely D_{ph} (photon component), D_n (neutron component), and D_{BNC} (BNC component), the following methods were employed. Pairwise microdosimetric spectra, with and without ^{10}B, were processed using the approach initially described by Wuu et al. [6]. The measurements were conducted using the TEPC in single-event modality, without evaluating the total absorbed dose. The dose probability distribution of the lineal energy, normalized to the unit dose, can be analyzed to derive the three dose components relative to the total. The photon component covers

the spectrum below approximately 20 keV/µm. The full distribution was obtained using a pure $yd(y)$ gamma spectrum aligned with the measured spectra, both with and without ^{10}B, to reconstruct the "e-edge region" (the shoulder in the photon part of the spectrum at about 10 keV/µm where the dose decreases). The subtraction of the photon component from the full $yd(y)$ distributions allows for the determination of the component due to neutrons. It should be noted that in the measurement with boron, the neutron component also encompasses the contribution of BNC events.

When comparing distributions measured with and without boron, normalization of the $d(y)$ distribution implies an adjustment of the height of the different components corresponding to their relative contribution to the total. However, the absolute dose contribution from non-thermal components of a mixed radiation field, particularly the gamma component, must remain the same. Taking this into account, the spectrum with boron was scaled by a constant factor to align its photon component with that of the distribution without ^{10}B. This scaling assumes that the presence of boron did not significantly alter this part of the spectrum, which is a reasonable approximation based on the very low boron content. Following the alignment of the photon component, the distribution without boron was then subtracted from the boron-inclusive distribution.

Finally, the obtained dose distributions $d(y)$ were used to calculate the relative biological effectiveness (RBE) of the radiation field, a crucial parameter in assessing the efficacy of therapeutic treatments. This calculation involved the application of the empirical weighting function, $r(y)$, determined by Tilikidis et al. at 2 Gy [25], to the dose lineal energy distributions, $d(y)$.

$$RBE = \int_{0.01}^{\infty} r(y)d(y)\mathrm{d}y \tag{3}$$

The Tilikidis weighting function at 2 Gy has been previously employed in microdosimetry of neutron fields for BNCT [17,26,27]. Estimating RBE through a single-response function offers a physics-based approach and facilitates intercomparisons between different BNCT facilities [28,29].

3. Results and Discussion

Figure 4 illustrates microdosimetric frequency distributions, represented as $yf(y)$, acquired under different boron concentrations and in the absence of boron. The left panel employs a logarithmic x-axis and a linear y-axis, ensuring that equivalent visual areas under the curves signify identical relative contributions to the total number of events. Notably, around half of the events exhibit lineal energy values below 0.15 keV/µm, with a minimal fraction surpassing 20 keV/µm. Specifically, this fraction is less than 0.1% without ^{10}B and rises to nearly 0.3% at a 100 ppm ^{10}B concentration.

When examining $yf(y)$ on a linear scale, the spectra with or without ^{10}B exhibit almost indistinguishable patterns, primarily due to the minor proportion of neutron-capture events involving boron compared to the total events. In the right panel of Figure 4, a double logarithmic scale is employed to accentuate small distinctions in events occurring above approximately 20 keV/µm. These variations arise from the increasing occurrence of BNC events as the boron concentration increases. Notably, the spectra maintain a consistent shape in the photon region (below 20 keV/µm), indicating minimal additional gamma components introduced by boron doping. This confirms the validity of the adopted procedure for aligning the photon components.

Figure 5 illustrates the dose distributions of the lineal energy at different boron concentrations. The distributions are graphed as $yd(y)$ vs. y, with the lineal energy y represented on a logarithmic scale. This graphical representation ensures that the size of the area under the curve between any two y values corresponds to the dose fraction in that range.

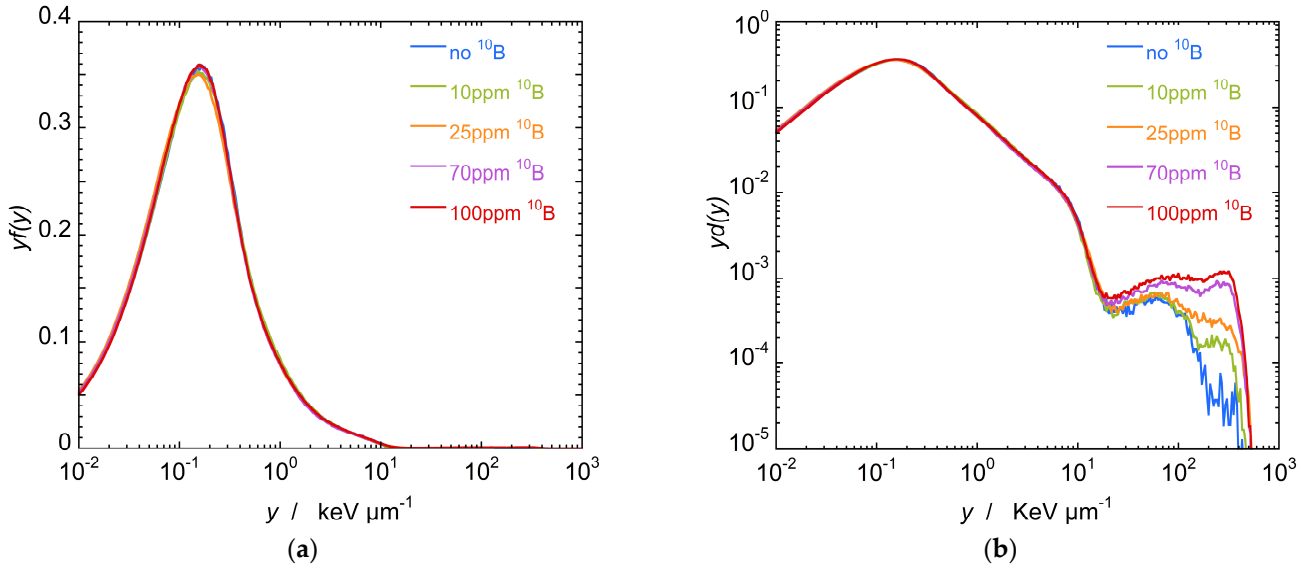

Figure 4. Frequency distributions of lineal energy with varying ^{10}B concentrations. (**a**) The logarithmic x-axis and a linear y-axis representation ensures that equal visual areas under the curves correspond to equal relative contributions to the total number of events; (**b**) the logarithmic vertical axis highlights variations in the spectrum's rightmost portion associated with the BNC reaction.

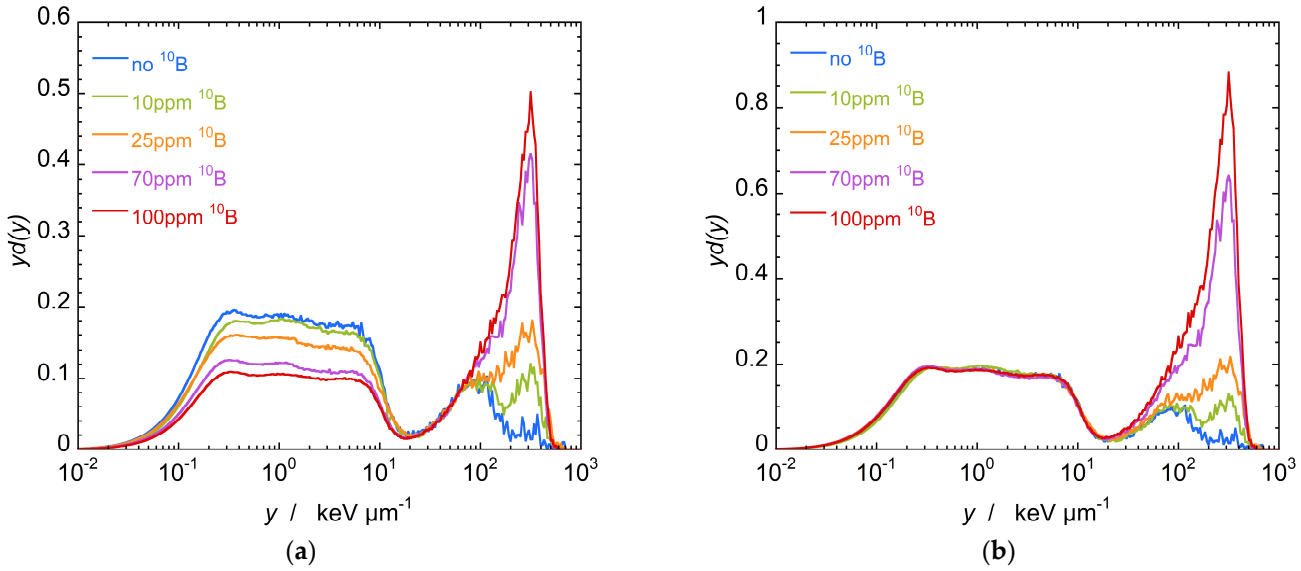

Figure 5. Dose distributions of lineal energy measured with different concentrations of ^{10}B. (**a**) All distributions have been normalized to a unit dose; (**b**) the dose distribution without ^{10}B is normalized to the unit dose, while the other distributions are scaled to align their gamma components, below 10 keV/μm, with the distribution without ^{10}B.

In the left panel of Figure 5, the $d(y)$ distributions are individually normalized to a unit dose, following the definition of the dose probability density of y, denoted as $d(y)$ [22]. As the high lineal energy components increase in the boronated spectra, the corresponding gamma components decrease to maintain normalization. It is important to note that this misalignment of the photon regions does not imply a reduction in gamma doses; instead, the gamma doses are expected to remain nearly the same. To address this, the photon regions (i.e., the part of the spectra below approximately 20 keV/μm) of the boronated spectra are aligned with the distribution without ^{10}B by scaling them with constant factors. This scaling, crucial for matching the gamma components, is a necessary step to accurately assess the additional contribution to the dose resulting from the boron neutron capture

reaction. Following proper scaling, the process enables the derivation of the pure BNC component by subtracting the boron-free spectrum from the one with boron.

As a result, the scaled $d(y)$ distributions for the boronated scenarios lose normalization. The excess beyond the unit dose, in the high-y region, reflects the dose fraction enhancement attributable to boron neutron capture reaction products.

In contrast to the similarities observed in the $f(y)$ distributions shown in Figure 4, the dose-weighted distributions displayed in Figure 5 exhibit significant differences. All spectra show a wide cluster of events, ranging from approximately 0.1 keV/µm to 20 keV/µm, originating from the interaction of photons with the detector walls. In the right panel of Figure 5, the shape of the photon component remains largely unaffected by the 0.48 MeV prompt gamma rays generated during BNC reactions. This occurs because this portion of the spectrum primarily arises from photons generated in the beamline, target, moderating structures, and (n,γ) reactions taking place on the detector wall materials, particularly hydrogen and aluminum.

The main differences are visible in the neutron component, above approximately 20 keV/µm. In the measurement without boron, two distinct peaks emerge. The first peak, spanning from 20 to 200 keV/µm, is attributed to recoil protons generated in the detector walls through fast neutron elastic scattering with hydrogen nuclei or the capture reaction of thermal neutrons on nitrogen. The second peak, extending from 200 to 500 keV/µm, originates from recoil light ions, predominantly constituted by recoil carbon ions generated when fast neutrons scatter within the cathode walls of the detector.

As the concentration of ^{10}B increases, the dose contribution above 20 keV/µm increases significantly as a result of the BNC reaction products. A substantial peak is formed with a maximum at approximately 300 keV/µm. Despite being responsible for a small fraction of all events, the BNC products make a significant contribution to the total absorbed dose when ^{10}B is added to the cathode walls. At a 100 ppm concentration of ^{10}B, the dose fraction corresponding to lineal energy events greater than 20 keV/µm amounts to approximately 50%.

Figure 6 reiterates the $yd(y)$ distributions, previously shown in the right panel of Figure 5, for the sake of enhanced visualization of the pure BNC components. In Figure 6, the BNC components are distinctly highlighted as colored lines. These BNC components were derived by subtracting the spectrum obtained without boron from the total spectra acquired with boronated walls. The areas under the colored curves in Figure 6 represent the relative dose enhancements resulting from the presence of ^{10}B. In addition to examining dose enhancements, we also calculated the relative enhancement in the total number of events. Both aspects, the relative enhancement in the number of events (left axis) and the absorbed dose (right axis), are depicted in Figure 7. This figure provides a comprehensive view of these enhancements as a function of the ^{10}B concentration in the cathode walls. It can be observed that both the frequency and the dose contributions of BNC events are proportional to the boron concentration, as expected. Any deviations from the anticipated proportionality are consistently less than 3%, as demonstrated in the bottom panel of Figure 7.

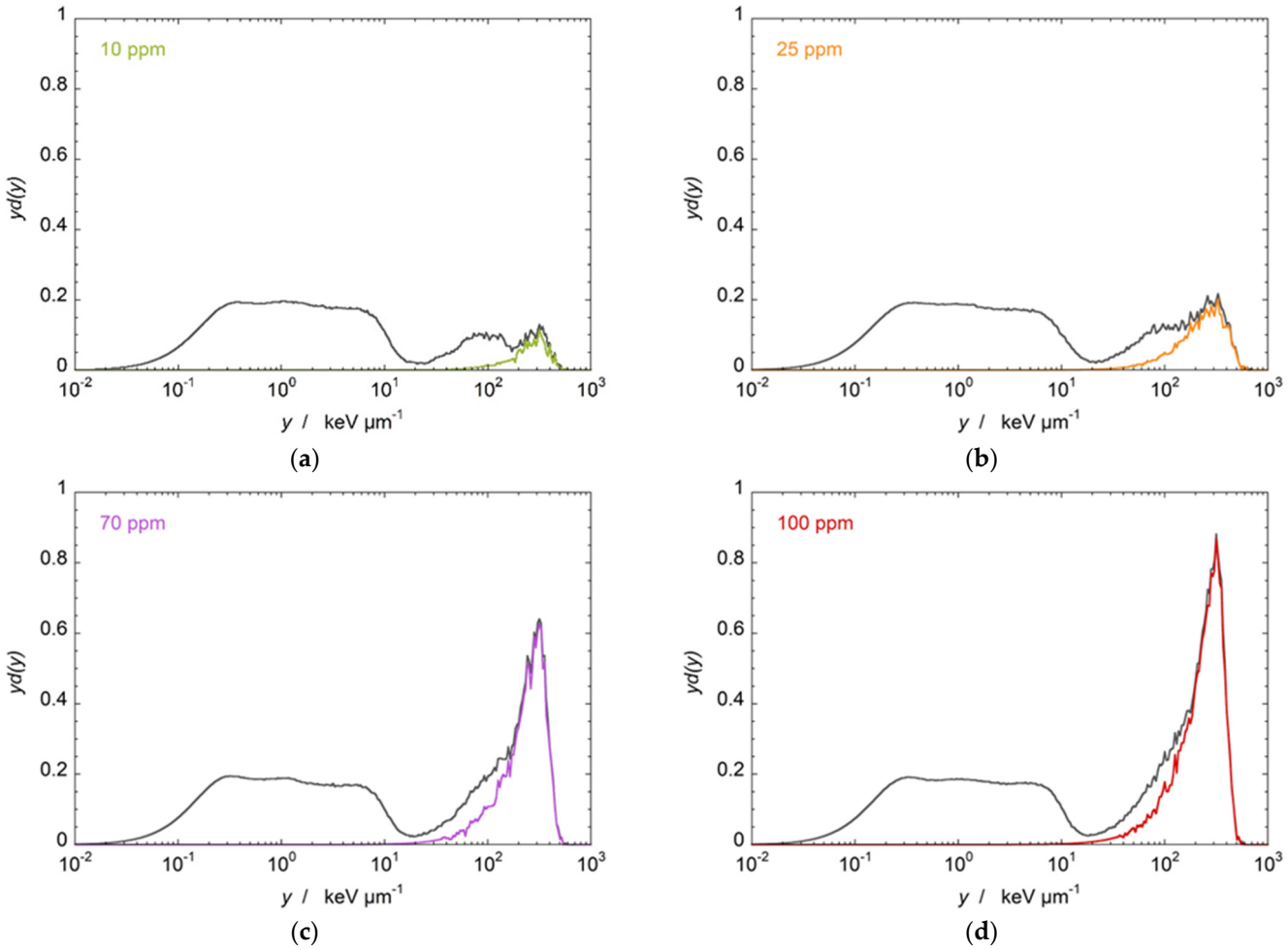

Figure 6. Microdosimetric $yd(y)$ distributions measured using cathode walls loaded with varying concentrations of ^{10}B. The solid black line represents the total distribution, encompassing both gamma and neutron components. In contrast, the colored lines represent the pure BNC components only. (**a**) 10 ppm of ^{10}B; (**b**) 25 ppm of ^{10}B; (**c**) 70 ppm of ^{10}B; (**d**) 100 ppm of ^{10}B.

Figure 8 shows the pure BNC components at the various boron concentrations. The red line at 100 ppm represents the measured data at 100 ppm. For other concentrations (10, 25, and 70 ppm), the thin lines represent data directly measured, while the thick lines were derived by scaling each value of the 100 ppm line. Specifically, each data point on the thick lines was calculated by multiplying the corresponding value of the 100 ppm line by the ratio of the actual boron concentration (X-ppm) to 100 ppm.

$$yd(y) \text{ at X-ppm} = yd(y) \text{ at 100 ppm} \times \frac{\text{X-ppm}}{\text{100-ppm}} \quad (4)$$

The agreement between the directly measured distributions (thin line) and the ones derived from the 100 ppm data (thick line) is excellent. The key point is that both the dose components and the spectral distribution at specific boron concentrations can be accurately derived from measurements at a single concentration, such as 100 ppm.

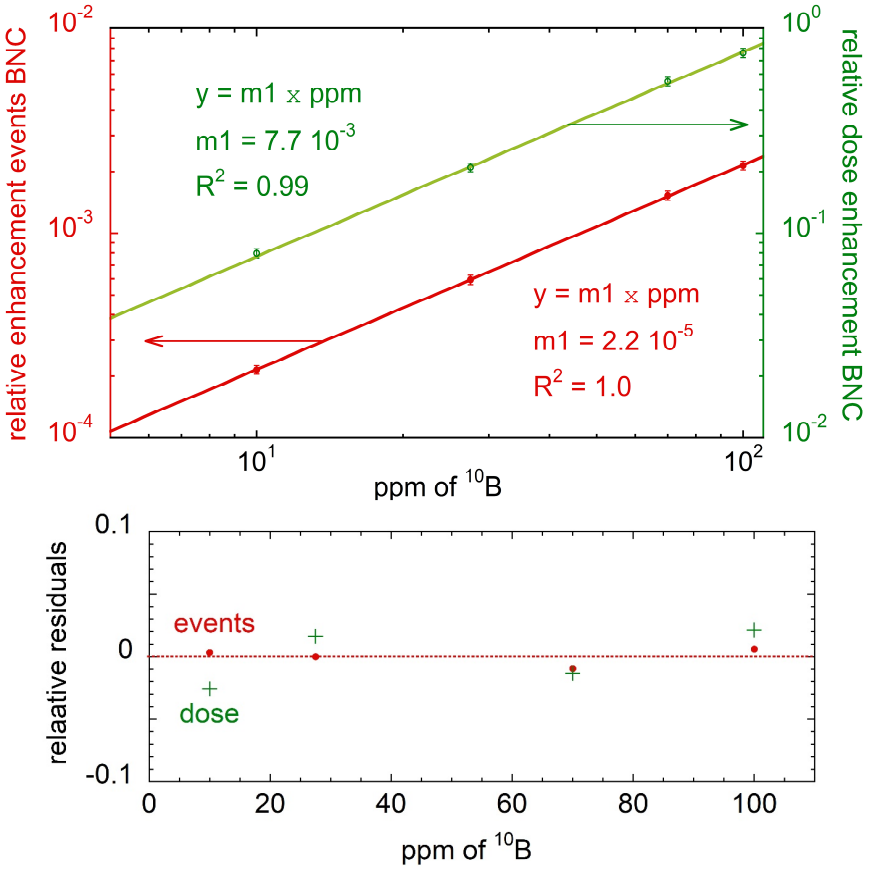

Figure 7. Top panel: the relative increase in the total number of events (red filled circles) and dose (green empty circles) as a function of ^{10}B concentration. Both enhancements are plotted relative to their values in the absence of ^{10}B. The lines are the linear best fit of experimental data (same colors as the symbols). **Bottom panel**: relative residuals with respect to a zero-intercept linear fit of experimental data.

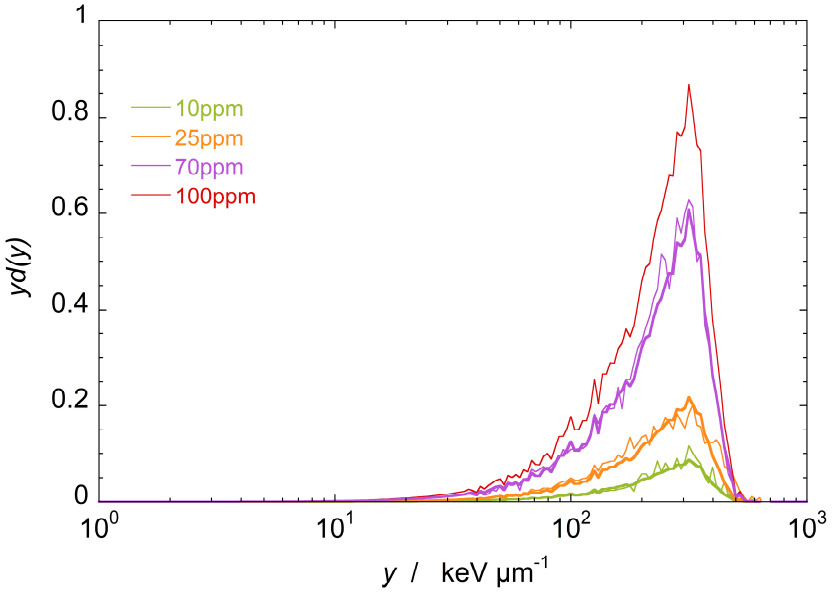

Figure 8. Microdosimetric BNC components of the $yd(y)$ distribution for cathode walls with varying concentrations of ^{10}B. The thin fluctuating lines represent the direct measurements. The thick lines represent the components evaluated at the concentrations of 10, 25, and 70 ppm of ^{10}B, scaling the single component measured at 100 ppm of ^{10}B.

Figure 9 depicts a comparison of the BNC component measured in this work at a simulated site size of 1 µm with the corresponding component measured and calculated by Wuu at a 2 µm site [6] and by Kota [10] and Burmeister at a 0.5 µm site [11]. The agreement between the curves is very good, and small discrepancies are consistent with the variations in site sizes, gas, and shape of the sensitive volume (SV).

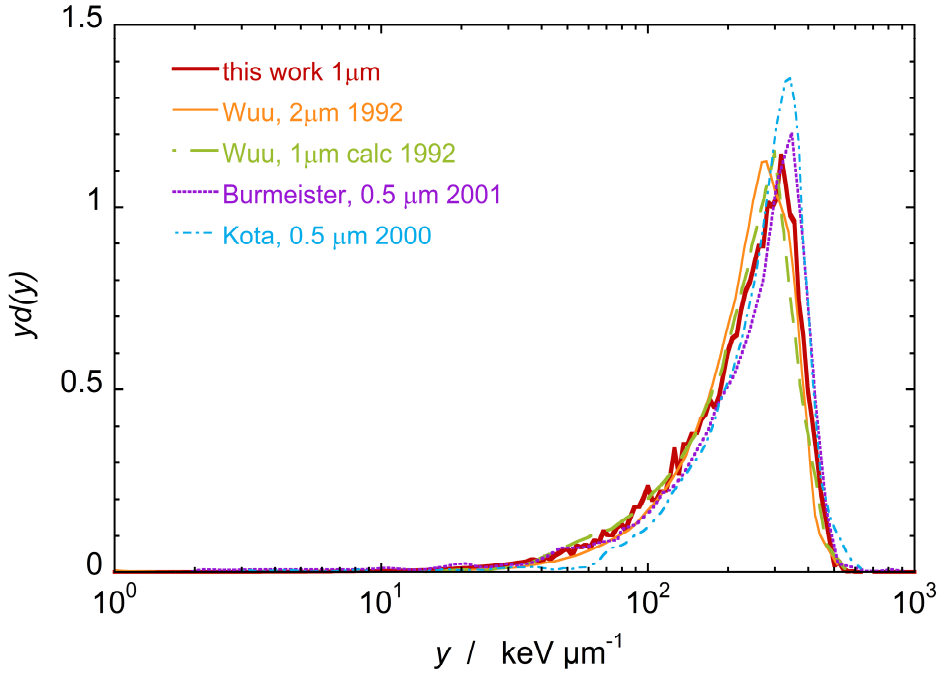

Figure 9. Microdosimetric BNC components of the $yd(y)$ distribution measured in this work, compared with those measured by Wuu [6], Kota [10] and Burmeister [11].

The three main relative dose components of the investigated radiation field, namely D_{ph}/D_{tot} (relative photon component), D_n/D_{tot} (relative neutron component), and D_{BNC}/D_{tot} (relative BNC component), at various boron concentrations, are reported in Table 1.

Table 1. The three main relative dose components at various ^{10}B concentrations.

^{10}B Concent/ppm	D_{ph}/D_{tot}	D_n/D_{tot}	D_{BNC}/D_{tot}
0	0.85	0.15	0
10	0.79	0.21	0.074
25	0.71	0.29	0.175
70	0.55	0.45	0.36
100	0.49	0.51	0.43

Spectral $yd(y)$ distributions were derived from the 100 ppm data for boron concentrations of 8.5 ppm and 30 ppm, representing typical average concentrations in BNCT for healthy and tumoral cells, respectively. These distributions are presented in Figure 10, along with the distribution without boron. The right panel of Figure 10 displays dose distributions weighted by the Tilikidis weighting function [25]. Application of the weighting function enhances the impact of the BNC component compared to the photon component. The absorbed dose, normalized to a nominal dose of 1 Gy delivered in the case of no boron enrichment, RBE values calculated using Equation (3), and the biological-weighted dose are reported in Table 2 for various boron concentrations.

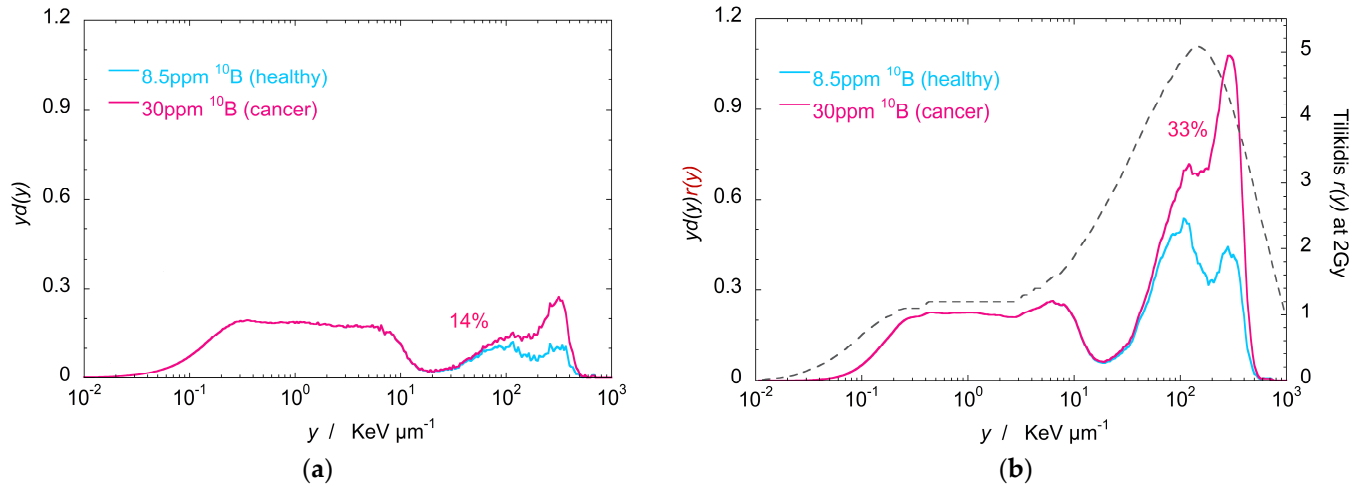

Figure 10. (**a**) Microdosimetric $yd(y)$ distributions measured with 0 ppm of ^{10}B, and reconstructed for a realistic scenario with 30 ppm of ^{10}B delivered to the tumor and 8.5 ppm to healthy tissue. (**b**) the $yd(y)r(y)$ distributions weighted with $r(y)$, the Tilikidis weighting function at 2 Gy, represented as a dotted line [25].

Table 2. The RBE, the relative physical dose, and RBE-weighted dose at several ^{10}B concentrations.

^{10}B Concent/ppm	RBE from Equation (3)	Absorbed Dose/Gy	RBE-Weighted Dose/Gy
0	1.68	1.00	1.68
8.5	1.87	1.08	2.02
10	1.88	1.08	2.03
25	2.12	1.20	2.55
30	2.19	1.23	2.68
70	2.65	1.55	4.10
100	2.85	1.76	5.01

It is worth noting that higher RBE values could potentially be attained by reducing the gamma component using appropriate shielding in the MUNES beam-shaping assembly.

Figure 10 illustrates that a differential boron concentration of 8.5 ppm in healthy tissue and 30 ppm in the tumor leads to a dose enhancement for cancer cells of approximately 14%. This enhancement is primarily attributed to high linear energy transfer (LET) alpha particles and Li ions, which have larger relative biological effectiveness (RBE) values. As a result, the RBE-weighted dose experiences a significant increase of 33%, playing a pivotal role in the curative effect of boron neutron capture therapy (BNCT).

The increase in the RBE-weighted dose could be further amplified by minimizing the gamma and fast neutron components, as these are not selectively targeted to cancerous tissue. In fact, the enhancement, confined to the region beyond 20 keV/µm, reaches a substantial 68%. It is important to note that the overall extent of enhancement depends on the contribution of the BNC component to the total dose—the higher the contribution of the BNC component, the greater the enhancement due to the selective delivery of boron. As highlighted in the IAEA report on BNCT [3], it is crucial to maintain control over radiation field components that cause non-selective dose absorption.

It is important to note that microdosimetry, performed with a homogeneous boron distribution in the cathode walls, represents a simplified version of the real scenario, where the micron-scale distribution of boron could be non-uniform. As highlighted by Green [30] and demonstrated through Monte Carlo simulations by Sato et al. [8], intra- and inter-cellular heterogeneity in ^{10}B distribution significantly impacts the biological effectiveness of boron neutron capture therapy (BNCT). Despite not precisely capturing the effects of a heterogeneous distribution, microdosimetry still offers valuable insights into the radiation field and the average impact of boron enrichment.

Furthermore, the microdosimetric characterization conducted using a gas detector with boron-enriched cathode walls reflects a scenario in which boron atoms are primarily externally delivered to the sensitive micrometric target. Even when working with boronated gas, the situation does not change significantly due to the low density of the gas compared to the walls. To explore a scenario where boron is included within the sensitive target, Monte Carlo simulations can be employed.

4. Conclusions

In this study, microdosimetric measurements were carried out using an avalanche-confinement tissue-equivalent proportional counter (TEPC), a specialized detector with interchangeable cathodes. Opting for this specific choice of TEPC provides the advantage that, aside from the boron content, all other characteristics of the detector remain exactly the same, allowing for a more controlled data processing.

Propane was used to fill the gas cavity at a pressure that simulated a 1 µm site size. The cathode walls were doped with varying concentrations of ^{10}B, ranging from 0 to 100 ppm. Pairwise measurements were performed, both with and without boron, to distinguish and isolate the gamma, neutron, and pure BNC components. We indirectly verified the nominal ^{10}B concentration, observing deviations from the nominal values of less than 3%. Additionally, we developed a robust procedure to extract the contribution of boron neutron capture (BNC) reactions for arbitrary ^{10}B concentrations. This experimental methodology allows for the use of microdosimetric measurements performed at an arbitrary boron concentration to predict the average effectiveness of boron uptake at any other concentration.

With the exception of publications from our research group at LNL, only the works of Wuu, Kota, and Burmeister provide experimental results that can be directly compared with the measurements conducted in this study, but the direct comparison is limited with regard to the boron neutron capture (BNC) component. This limitation arises because the radiation fields were not the same, and components other than the BNC are strongly dependent on the radiation field composition and detector characteristics (e.g., wall thickness). The comparison with the BNC components measured by Wuu, Kota, and Burmeister is very good, with small discrepancies that are consistent with the different experimental conditions.

Despite the limitations relative to the boron distribution within and around the biological target, which were mentioned in the discussion, the microdosimetric approach provides valuable insights into the biological effects of BNCT on cancerous and healthy tissues, contributing to the development of innovative treatment strategies. Potential applications of microdosimetry include, for instance, the implementation of experimental microdosimetric spectra, measured at different depths in phantom, as input data of advanced treatment planning [31,32].

It is crucial to emphasize that the microdosimetric component of boron neutron capture (BNC), measured using the TEPC method, corresponds to the cellular effect when ^{10}B atoms are situated in the tissue surrounding the biological sensitive target, rather than within it. Since the BNC dose is released inside the cell by two ions emitted simultaneously at an angle of 180°, the TEPC, by design, captures ionization events resulting from only one of the two ions produced in the A-150 walls. Consequently, the event size measured by the TEPC is generally smaller than the event size produced by a BNC reaction inside the biological target. To further explore the impact of different boron atom placements within biological tissue at micrometer scale, including a heterogeneous distribution, we recommend conducting Monte Carlo simulations. TEPC measurements can serve as a valuable tool to validate the Monte Carlo model.

Author Contributions: Conceptualization, V.C.; methodology, V.C., A.B. and A.S.; data analysis, V.C.; writing—original draft preparation, V.C.; writing—review and editing, A.B. and A.S. All authors have read and agreed to the published version of the manuscript.

Funding: This work was supported by the Fifth Scientific Commission of the Italian National Institute for Nuclear Physics (INFN).

Institutional Review Board Statement: Not applicable.

Informed Consent Statement: Not applicable.

Data Availability Statement: Raw data were generated at Legnaro National Laboratories of INFN. The data presented in this study are available in article.

Acknowledgments: Authors acknowledge Paolo Colautti for the experimental support, valuable discussions, and insightful guidance provided during this study.

Conflicts of Interest: The authors declare no conflict of interest. The funders had no role in the design of the study; in the collection, analyses, or interpretation of data; in the writing of the manuscript; or in the decision to publish the results.

References

1. Locher, G.L. Biological effects and therapeutic possibilities of neutrons. *Am. J. Roentgenol. Radium Ther.* **1936**, *36*, 1–13.
2. Farr, L.E.; Sweet, W.H.; Locksley, H.B.; Robertson, J.S. Neutron capture therapy of gliomas using boron-10. *Trans. Am. Neurol. Assoc.* **1954**, *79*, 110–113.
3. International Atomic Energy Agency. *Current Status of Neutron Capture Therapy*; IAEA-TECDOC-1223; International Atomic Energy Agency: Vienna, Austria, 2001.
4. International Atomic Energy Agency. *Advances in Boron Neutron Capture Therapy*; Non-Serial Publications, IAEA, CRCP/BOR/002; International Atomic Energy Agency: Vienna, Austria, 2023; ISBN 978-92-0-132723-9.
5. Coderre, J.A.; Morris, G.M. The radiation biology of boron neutron capture therapy. *Radiat. Res.* **1999**, *151*, 1–18. [CrossRef] [PubMed]
6. Wuu, C.S.; Amols, H.I.; Kliauga, P.; Reinstein, L.E.; Saraf, F. Microdosimetry for boron neutron capture therapy. *Radiat. Res.* **1992**, *130*, 355. [CrossRef] [PubMed]
7. Zamenhof, R.G. Microdosimetry for boron neutron capture therapy: A review. *J. Neurooncol.* **1997**, *33*, 81. [CrossRef]
8. Sato, T.; Masunaga, S.; Kumada, H.; Hamada, N. Microdosimetric Modeling of Biological Effectiveness for Boron Neutron Capture Therapy Considering Intra- and Intercellular Heterogeneity in ^{10}B Distribution. *Sci. Rep.* **2018**, *8*, 988. [CrossRef] [PubMed]
9. Hu, N.; Tanaka, H.; Takata, T.; Endo, S.; Masunaga, S.; Suzuki, M.; Sakurai, Y. Evaluation of PHITS for microdosimetry in BNCT to support radiobiological research. *Appl. Radiat. Isot.* **2020**, *161*, 109148. [CrossRef] [PubMed]
10. Kota, C.; Maughan, R.; Tattam, D.; Beynon, D. The use of low pressure tissue equivalent proportional counters for the dosimetry of neutron beams used in BNCT and BNCEFNT. *Med. Phys.* **2000**, *27*, 535. [CrossRef]
11. Burmeister, J.; Kota, C.; Maughan, R.L.; Waker, A. Miniature tissue equivalent proportional counters for BNCT and BNCEFNT dosimetry. *Med. Phys.* **2001**, *28*, 1911. [CrossRef]
12. Burmeister, J.; Riley, K.; Coderre, J.; Harling, O.; Ma, R.; Wielopolski, L.; Kota, C.; Maughan, R. Microdosimetric intercomparison of BNCT beams at BNL and MIT. *Med. Phys.* **2003**, *30*, 2131. [CrossRef]
13. De Nardo, L.; Seravalli, E.; Rosi, G.; Esposito, J.; Colautti, P.; Conte, V.; Tornielli, G. BNCT microdosimetry at the TAPIRO reactor thermal column. *Radiat. Prot. Dosim.* **2004**, *110*, 579. [CrossRef] [PubMed]
14. Hsu, F.Y.; Hsiao, H.W.; Tung, C.J.; Liu, H.M.; Chou, F.I. Microdosimetry study of THOR BNCT beam using tissue equivalent proportional counter. *Appl. Radiat. Isot.* **2009**, *67*, S175. [CrossRef] [PubMed]
15. Moro, D.; Colautti, P.; Lollo, M.; Esposito, J.; Conte, V.; De Nardo, L.; Ferretti, A.; Ceballos, C. BNCT dosimetry performed with a mini twin tissue-equivalent proportional counter (TEPC). Appl. *Radiat. Isot.* **2009**, *67*, S171. [CrossRef] [PubMed]
16. Colautti, P.; Moro, D.; Chiriotti, S.; Conte, V.; Evangelista, L.; Altieri, S.; Bortolussi, S.; Protti, N.; Postuma, I. Microdosimetric measurements in the thermal neutron irradiation facility of LENA reactor. *Appl. Radiat. Isot.* **2014**, *88*, 147. [CrossRef] [PubMed]
17. Selva, A.; Bellan, L.; Bianchi, A.; Giustiniani, G.; Colautti, P.; Fagotti, E.; Pisent, A.; Conte, V. Microdosimetry of an accelerator based thermal neutron field for Boron Neutron Capture Therapy. *Appl. Radiat. Isot.* **2022**, *182*, 110144. [CrossRef]
18. Cesari, V.; Colautti, P.; Magrin, G.; De Nardo, L.; Baek, W.Y.; Grosswendt, B.; Alkaa, A.; Khamphan, C.; Segur, P.; Tornielli, G. Nanodosimetry measurements with an avalanche confinement TEPC. *Radiat. Prot. Dosim.* **2002**, *99*, 337. [CrossRef] [PubMed]
19. Ceballos, C.; Esposito, J.; Agosteo, S.; Colautti, P.; Conte, V.; Moro, D.; Pola, A. Towards the final BSA modeling for the accelerator-driven BNCT facility at INFN LNL. *Appl. Radiat. Isot.* **2011**, *69*, 1660. [CrossRef]
20. Agosteo, S.; Colautti, P.; Esposito, J.; Fazzi, A.; Introini, M.V.; Pola, A. Characterization of the energy distribution of neutrons generated by 5 MeV protons on a thick beryllium target at different emission angles. *Appl. Radiat. Isot.* **2011**, *69*, 1664. [CrossRef]
21. Chiriotti, S.; Moro, D.; Colautti, P.; Conte, V.; Grosswendt, B. Equivalence of pure propane and propane-TE gases for microdosimetric measurements. *Radiat. Prot. Dosim.* **2015**, *166*, 242. [CrossRef]
22. International Commission on Radiation Units and Measurements. *Microdosimetry Report 36*; International Commission on Radiation Units and Measurements: Bethesda, MD, USA, 1983.

23. Bianchi, A.; Mazzucconi, D.; Selva, A.; Colautti, P.; Parisi, A.; Vanhavere, F.; Reniers, B.; Conte, V. Lineal Energy Calibration of a Mini-TEPC via the Proton-Edge Technique. *Radiat. Meas.* **2021**, *141*, 106526. [CrossRef]
24. Bianchi, A.; Selva, A.; Colautti, P.; Parisi, A.; Vanhavere, F.; Reniers, B.; Conte, V. The effect of different lower detection thresholds in microdosimetric spectra and their mean values. *Radiat. Meas.* **2021**, *146*, 106626. [CrossRef]
25. Tilikidis, A.; Lind, B.; Näfstadius, P.; Brahme, A. An estimation of the relative biological effectiveness of 50 MV bremsstrahlung beams by microdosimetric techniques. *Phys. Med. Biol.* **1996**, *41*, 55. [CrossRef] [PubMed]
26. Endo, S.; Onizuka, Y.; Ishikawa, M.; Takada, M.; Sakurai, Y.; Kobayashi, T.; Tanaka, K.; Hoshi, M.; Shizuma, K. Microdosimetry of neutron field for boron neutron capture therapy at Kyoto University reactor. *Radiat. Protect. Dosim.* **2004**, *110*, 641–644. [CrossRef] [PubMed]
27. Endo, S.; Tanaka, K.; Fujikawa, K.; Horiguchi, T.; Itoh, T.; Onizuka, Y.; Hoshi, M.; Murataka, A.; Kojima, Y.; Shizuma, K. Microdosimetry on a mini-reactor UTRKINKI for educational uses and biological researches. *J. Radiat. Res.* **2009**, *50*, 83–87. [CrossRef] [PubMed]
28. Wambersie, A. Contribution of microdosimetry to the specification of neutron beam quality for the choice of the "clinical RBE" in fast neutron therapy. *Rad. Prot. Dosim.* **1994**, *52*, 453. [CrossRef]
29. Gueulette, J.; Octave-Prignot, M.; De Coster, B.-M.; Wambersie, A.; Grégoire, V. Intestinal crypt regeneration in mice: A biological system for quality assurance in non-conventional radiation therapy. *Radiother Oncol.* **2004**, *73*, S148–S154. [CrossRef]
30. Green, S. Comments on 'A microdosimetric study of the dose enhancement in a fast neutron beam due to boron capture'. *Phys. Med. Biol.* **1994**, *39*, 923–924. [CrossRef]
31. Sato, T.; Furusawa, Y. Cell Survival Fraction Estimation Based on the Probability Densities of Domain and Cell Nucleus Specifc Energies Using Improved Microdosimetric Kinetic Models. *Radiat. Res.* **2012**, *178*, 341–356. [CrossRef]
32. Hu, N.; Tanaka, H.; Takata, T.; Okazaki, K.; Uchida, R.; Sakurai, Y. Microdosimetric quantities of an accelerator-based neutron source used for boron neutron capture therapy measured using a gas-filled proportional counter. *J. Radiat. Res.* **2020**, *61*, 214. [CrossRef]